Natural Hazards and Earth System Sciences

Open Access

Discussions

Improvement of shallow landslide prediction accuracy using soil parameterisation for a granite area in South Korea

M. S. Kim[1], Y. Onda[1], and J. K. Kim[2]

[1]Department of Integrative Environmental Sciences, Graduate School of Life and Environmental Sciences, University of Tsukuba, Tsukuba 305-8572, Japan
[2]Quaternary Geology Research Department, Korea Institute of Geoscience and Mineral Resources (KIGAM), 124 Gwahang-no, Yuseong-gu, Daejeon 305-350, Republic of Korea

Correspondence to: J. K. Kim (jinkwankim77@gmail.com)

Abstract

SHALSTAB model applied to shallow landslides induced by rainfall to evaluate soil properties related with the effect of soil depth for a granite area in Jinbu region, Republic of Korea. Soil depth measured by a knocking pole test and two soil parameters from direct shear test (a and b) as well as one soil parameters from a triaxial compression test (c) were collected to determine the input parameters for the model. Experimental soil data were used for the first simulation (Case I) and, soil data represented the effect of measured soil depth and average soil depth from soil data of Case I were used in the second (Case II) and third simulations (Case III), respectively. All simulations were analysed using receiver operating characteristic (ROC) analysis to determine the accuracy of prediction. ROC analysis results for first simulation showed the low ROC values under 0.75 may be due to the internal friction angle and particularly the cohesion value. Soil parameters calculated from a stochastic hydro-geomorphological model were applied to the SHALSTAB model. The accuracy of Case II and Case III using ROC analysis showed higher accuracy values rather than first simulation. Our results clearly demonstrate that the accuracy of shallow landslide prediction can be improved when soil parameters represented the effect of soil thickness.

1 Introduction

Climate change has increased rainfall intensity in some regions, resulting in increased landslide occurrence. The increasing frequency and magnitude of landslides have been studied in mountainous areas worldwide due to the potential impact on human life (Selby, 1976; Eyles et al., 1978; Guthrie, 2002). Rainfall-induced shallow landslides have been studied for practical and scientific reasons (Anderson and Sitar, 1995; Iverson et al., 1997; Gabet and Muss, 2006). Regardless of the various scales of shallow landslides, they pose a significant hazard to mountain communities because they are frequent and difficult to predict, and they can develop into debris flows that are poten-

tially destructive due to their velocity and potential for sediment bulking during propagation (Campbell, 1975; Rickenmann and Zimmermann, 1993; Iverson et al., 1997; Reid et al., 2000; Crosta and Dal Negro, 2003; Crosta et al., 2003).

The initiation of shallow landslides is often related to rainfall intensity and duration (Caine, 1980; Aleotti, 2004; Giannecchini et al., 2006, 2007; Guzzetti et al., 2007, 2008; Cannon et al., 2008; Coe et al., 2008). It has been frequently observed that hillslope failures such as shallow landslides are often related to short ($< 1\,\text{h}$) and intense rainfall rather than daily-averaged precipitation (Reid et al., 1997; Montgomery et al., 1997; Caine, 1980; Casadei et al., 2003). Previous rainfall, geological soil properties, soil thickness, and hydraulic conductivity play important roles in triggering landslides, and the rate of water infiltration and water movement below the surface are also important factors for landslide initiation (Iverson, 2000; Crosta and Frattini, 2003; Giannecchini et al., 2007).

Recent physically based models have revealed the amount of precipitation required to trigger slope failures and the locations and times of the expected landslides, making these models of interest for landslide warning systems. Others combine an instability model with a hydrological model to provide better general models for topographically controlled shallow slope failures (Montgomery and Dietrich, 1994; Dietrich et al., 1995; Casadei et al., 2003). Many shallow landslide modelling efforts have focused on more effective ways to describe flows from upslope using topographic index or dynamic topographic index approaches (i.e., Montgomery and Dietrich, 1994; Tarolli and Tarboton, 2006). However, these physically based models only allow complete parameterisations and do not consider rainfall-induced landslides where definitions are needed for components such as the hydrological response of the soil and its geotechnical properties (Giannecchini et al., 2007). The infinite-slope concept in a physically based model analysis is usually adopted within the defined physical parameters of the study area, and data of the in situ spatial distribution of soil thickness are required to perform slope instability analysis.

Soil thickness is of particular importance, as are the mechanical and hydrological properties related to hydraulic conductivity, transmissivity, and the angle of internal friction. A uniform soil thickness was used in previous analyses of shallow landslides (e.g., Montgomery and Dietrich, 1994; Dietrich et al., 1995; Wu and Slide, 1995), and some researchers included sparse soil thickness sampling data in the analysis of shallow landslides. Recently, however, Lee and Ho (2009) adopted the wetness index to determine the spatial distribution of soil thickness for slope instability analysis. Ho et al. (2012) also applied uniformly distributed soil thicknesses to assess the success rate for physically based shallow landslide prediction using different soil thickness assumptions for comparison.

Various soil factors such as vegetation, roots, and internal friction angle can also affect the occurrence of shallow landslides. Kuriakose et al. (2009) attempted to evaluate the sensitivity of slope stability to the hydrological effects of vegetation and root reinforcement together with other intrinsic and extrinsic factors in their research area using a dynamic hydrological model combined with a slope stability model. Sidle and Ochiai (2006) noted that shallow landslides were affected by the internal friction angle of soil where the slope gradient is greater than the angle of internal friction of the failure surface.

Researchers have variously attributed the seemingly random occurrence of landslides to spatial variation in topography, soil depth, cohesion of the soil and roots, hydraulic conductivity, groundwater response, and the angle of internal friction (e.g., Dietrich et al., 1995; Wu and Sidle, 1995; Montgomery et al., 1997). Unfortunately, these variables are exceedingly difficult to measure, and few studies have attempted to measure their spatial variation at the scale that influences slope stability. Although several researchers (Dietrich et al., 1995; Claessens et al., 2005; Rosso et al., 2006; Uchida et al., 2011) have observed that soil properties are important factors for shallow landslide modelling performance and have incorporated these factors into their work, studies considering changes in the physical characteristics of soil with varying thickness remain rare. Shallow landslide prediction could be affected by various char-

acteristics of the study area, especially including the frequency of the past landslide, slope steepness, soil properties, forest cover, and timing of past landslides.

In this context, Korea is the ideal field site to test the performance of the landslide model because the occurrence of shallow landslides is just accelerated by the recently
5 increased heavy rainstorms. Therefore, we did not need to consider the impact of the recent landslides. We performed predictions of shallow landslides induced by rainfall by using a SHALSTAB model (Dietrich et al., 1995; Dietrich and Montgomery, 1998; Montgomery and Dietrich, 1994; Montgomery et al., 1998) and interpreted the importance of soil parameters such as cohesion and internal friction angle according to changes in
10 soil thickness to improve the accuracy of shallow landslide prediction in Jinbu-Myeon, Pyeongchang-gun, Kangwon Prefecture in the Republic of Korea. We used a knocking pole test in the study area where landslides are increasing, recently to measure soil thickness data and, the three soil parameters, which were collected at study area and analysed using two methods (direct shear tests and one triaxial compression test),
15 used in SHALSTAB model.

2   Study area

The approximately $70 \, \text{km}^2$ study area is located in Jinbu-Myeon, Pyeongchang-gun, Kangwon Prefecture in the Republic of Korea; the centre of the study area is located at $128°33'29''$ E, $37°37'49''$ N (Fig. 1). The annual mean precipitation in this area during
20 the last 40 years (1978–2008) was about 1400 mm (Korea Meteorological Agency). This region has a temperate climate with year-round precipitation. Rainfall primarily occurs during the summer season, from June to September, as part of the East Asian monsoon. Korea is also threatened by severe tropical typhoons during the summer season. Most of the heavy rainfall observed in Korea can be attributed to typhoon
25 activity in the area. On 16 July 2006, over 1200 shallow landslides occurred in the Jinbu region as a result of typhoon rains. The Korea Meteorological Administration

measured the total rainfall amount at 450 mm day^{-1} and the maximum rainfall intensity of the triggering event at about 45 mm h^{-1}.

The prevalent geological units exposed in the study area are the Mesozoic Nokam Formation and igneous rocks including the Imgye granite. The Triassic Nokam Formation is composed of fine sandstone with grey sandy shale, originating from thick clastic successions of marginal marine to nonmarine environments. In contrast, the Jurassic plutonic rock, the Imgye granite, mainly occurs as a large batholith trending NW–SE and as small stocks consisting of granite with minor syenite and diorite distributed along the Ogcheon Belt. Additionally, the Ordovician Jeongseon limestone is mainly of shallow marine origin and consists predominantly of limestone with lesser amounts of sandstone and shale. This area has undergone extensive intrusion by granitoids due to the Daebo Orogeny, which lasted from the early Jurassic to the early Cretaceous. All of the previous geological units were intensely deformed as a result of this intense orogenic event (Hong et al., 1995; Park et al., 2013).

3 Methods

3.1 Critical rainfall calculation

We used a SHALSTAB model combined with infinite slope stability equation and simple subsurface flow model for the shallow landslide hazard analysis (Fig. 2). This method was described by Montgomery and Dietrich (1994) and is based on earlier formulations proposed by O'Loughlin (1986). The practicality of this approach and various adaptations of it have been demonstrated over the last decade, and it performs well for many applications (Dietrich et al., 1995; Dietrich and Montgomery, 1998; Wu and Sidle, 1995; Borga et al., 2002; Montgomery et al., 2000; Pack et al., 2001; Vanacker et al., 2003; Fernandes et al., 2004). Calculation of the R_c (slope stability index; Eq. 1) is based on the infinite slope form of the Mohr–Coulomb failure law, expressed by the ratio of the stabilising force (shear strength) to the destabilising force (shear stress) on a failure

plane parallel to the ground surface (e.g., Montgomery and Dietrich, 1994; Dietrich and Montgomery, 1998).

$$R_c = T \sin \beta \left(\frac{b}{a} \right) \left(\frac{\rho_s}{\rho_w} \right) \left[1 - \frac{(\sin \beta - C)}{(\cos \beta \tan \varnothing)} \right] \tag{1}$$

where T is the saturated soil transmissivity ($m^2 h^{-1}$), β is the local slope angle (°), θ is the internal friction angle of the soil (°), a is the upslope contributing area (m^2), b is the unit contour length (in our grid-based approach the grid resolution (m) is taken as the effective contour length, as in Pack et al., 2001), ρ_s is the wet soil bulk density ($g\,cm^{-3}$), and ρ_w is the density of water ($g\,cm^{-3}$). C is the combined cohesion term (−), made dimensionless relative to the perpendicular soil thickness and defined as

$$C = \frac{C_r + C_s}{h \rho_s g} \tag{2}$$

where C_r is the root cohesion (Nm^{-2}), C_s is the soil cohesion (Nm^{-2}), h is the perpendicular soil thickness (m), and g is the gravitational acceleration constant ($9.81\,m\,s^{-2}$). Given the assumptions and boundary conditions used in deriving Eq. (1), it could be expressed using the conditions for the upper and lower thresholds of elements that can possibly fail. Unconditionally stable areas are predicted to be stable even when saturated, and they satisfy

$$\tan \theta \leq \left(\frac{C}{\cos \theta} \right) + \left(1 - \frac{\rho_s}{\rho_w} \right) \tan \varnothing \tag{3}$$

Unconditionally unstable elements, which in most cases are bedrock outcrops, are unstable even when dry, and they satisfy

$$\tan \theta > \tan \varnothing + \left(\frac{C}{\cos \theta} \right) \tag{4}$$

Title Page

Abstract | Introduction

Conclusions | References

Tables | Figures

|◄ | ►|

◄ | ►

Back | Close

Full Screen / Esc

Printer-friendly Version

Interactive Discussion

The predictive index of this model (i.e., the stability index) is expressed in mm day^{-1} of critical rainfall and is of variable scale, where lower values indicate a higher probability of instability, and higher values indicate a greater probability of stability. This scale also encompasses areas identified as unconditionally stable and unconditionally unstable
5 based on the estimated rainfall value (Zizioli et al., 2013).

3.2 Stochastic model for soil parameterisation

Topography influences the initiation of shallow landslides through both the concentration of subsurface flow and the effects of slope gradient on slope stability (Montgomery and Dietrich, 1994; Talebi et al., 2008). Slope failure often occurs in areas of con-
10 vergent topography, where subsurface soil water flow paths increase the excess pore water pressure downslope (Anderson et al., 1991; Wilkinson et al., 2002; Talebi et al., 2008). Planar infinite slope analysis has been widely applied to the evaluation of natural slope stability, particularly where the thickness of the soil mantle was small relative to slope length and where shallow landslides occurred due to the failure of a soil mantle
15 overlying a sloping drainage barrier (Talebi et al., 2008). Iida (1999) suggested that the two-layer model of soil and bedrock, which assumes a potential landslide (soil) layer, is suitable for the slope stability analysis of shallow landslides. Several researchers (Iida, 1999; D'Odorico and Fragherazzi, 2002; Talebi et al., 2008) applied the same approach in a stochastic hydrogeomorphological model for shallow landslides resulting
20 from rainstorms. This model is based on the Mohr–Coulomb failure law, and the failure condition can be expressed as (Iida, 1999)

$$H_{cr} = \frac{c - \gamma_t \cos^2 \beta (\tan \beta - \tan \varnothing) D}{\cos^2 \beta \{(\gamma_{sat} - \gamma_t)(\tan \beta - \tan \varnothing) + \gamma_w \tan \varnothing\}} \tag{5}$$

where β is the local slope angle (°), c is the cohesion, $\varnothing$ is the internal friction angle (°), γ_t is the weight per unit volume of unsaturated soil (g cm^{-3}), γ_{sat} is the weight per

234

unit volume of saturated soil ($g\,cm^{-3}$), and γ_w is the weight of water per unit volume ($g\,cm^{-3}$).

In this model, shallow landslides occur when the soil thickness D is between D_{cr} and D_{max} (Talebi et al., 2008).

⁵ When the soil Depth D is equal to D_{cr}, the critical soil depth D_{cr} can be expressed as follows:

$$D_{cr} = c/\cos^2\beta \{\gamma_{sat}(\tan\beta - \tan\varnothing) + \gamma_w \tan\varnothing\} \tag{6}$$

When the soil depth D is less than D_{max} ($D_{max} > D$), the depth D of saturated through-flow cannot reach the critical D_{cr} value, even in a rainstorm. Thus, shallow landslides do ¹⁰ not occur because the water table of the saturated throughflow cannot rise above the ground surface, resulting in saturated overland flow. In the case of a relatively steep slope ($\varnothing < \beta$), D_{cr} decreases linearly with increased soil depth D, and D_{cr} becomes zero. This means that a shallow landslide can occur on the slope without saturated throughflow, given a critical ("upper limit") soil depth D.

¹⁵ $$D_{max} = c/\gamma_t \cos^2\beta(\tan\beta - \tan\varnothing) \tag{7}$$

The modelling soil of evolution is important because without cohesion, soils could never form on slopes greater than $\varnothing$, and even thin soils on slopes in the range of $\beta < \varnothing$ would be extremely unstable because light rainfall would provide a sufficient saturated water depth H to cause landslides. These scenarios are contrary to observation, suggesting ²⁰ that soil cohesion must be considered in slope stability models (Iida, 1999).

3.3 Model input parameterisations

Unsaturated and saturated subsurface flow on hillslopes and/or catchments is affected by topography, soil depth, and hydraulic properties in a complex manner. These properties serve as input data for numerical simulations and have significant implications for

simulation accuracy. Although detailed surface topography data can generally be readily obtained from digital elevation models (DEMs), soil depth and hydraulic properties for an entire hillslope and/or catchment are often lacking. The topographic data used in this study consisted of a 5 m × 5 m DEM based on a digital elevation map (1 : 5000) from the National Geographic Information Institute in the Republic of Korea. The locations of shallow landslide areas were back-filled to represent the topography of the study area before the landslides occurred.

The dynamic cone penetrometer (25 mm diameter with a 60° tip angle), also known as the knocking pole (Yoshinaga and Ohnuki, 1995), consists of several 0.5 m sections of 15 mm-diameter stainless steel rods with graduations etched every 10 cm. The penetration resistance value, Nd (drop/10 cm), was computed as the number of blows required for 10 cm penetration. Uchida et al. (2009) compared vertical Nd distributions among locations outside and inside areas of shallow slope failure and found that soil layers with Nd values of 5–20 were not detected as locations within areas of slope failure in their study area. They suggested that soil depths with Nd $\leq$ 20 could be defined as soil layers with failure potential, and soil depths with Nd $\geq$ 20 could be defined as bedrock layers not prone to failure. For our study, 125 penetration tests were performed at 10–15 m intervals along the slope, and the soil distribution was calculated using the Nd values (Fig. 1b). To compare actual shallow landslides with our shallow landslide simulation results, we used air photo images taken after shallow landslide occurrence and converted the shallow landslide area into polygons using the ArcGIS 10.1 program (ESRI, California, USA).

We collected soil samples from the study area and tested them using a triaxial compression test to determine the model input parameters. Testing soils to understand their behaviour during shallow failures normally requires a method that mimics the stress distribution under natural conditions. Shallow landslides are triggered by elevated pore pressure that decreases the effective normal stress rather than by increasing shear stress (Anderson and Reimer, 1995). Unlike typical triaxial shear testing that is accomplished by increasing the shear stress, the consolidated drained (CD) test approximates

Improvement of shallow landslide prediction accuracy using soil parameterisation

M. S. Kim et al.

Title Page

Abstract | Introduction

Conclusions | References

Tables | Figures

⏮ | ⏭

◀ | ▶

Back | Close

Full Screen / Esc

Printer-friendly Version

Interactive Discussion

the conditions during rainfall-induced failure by maintaining constant shear stress while reducing the effective stress (Reimer, 1992). Lee et al. (2009) and Park et al. (2013) tested soil samples at the same study site for soil parameters using a direct shear test, and we used soil data from these studies, which were performed in the study area
5 (Table 1).

3.4 Assessment of model results

The prediction accuracy of regional landslide susceptibility models has typically been evaluated by comparing the locations of the known landslides with simulation results from the model (Montgomery et al., 1998, 2001; Godt et al., 2008). Receiver operating
10 characteristics (ROCs), which are used in various studies including weather forecasting and landslide susceptibility mapping, represent a technique for comparing the performance of models for which results can be assigned to one of two classes or states (Swets, 1988; Fawcett, 2006; Van Den Eeckhaut et al., 2006; Godt et al., 2008). The model with the higher percentage provides a better prediction of shallow landslides.
15 The least critical test of prediction accuracy would be to count a successful prediction when a single grid cell is located within a mapped landslide polygon.

   More critical tests of prediction accuracy involve more detailed assessment of (1) the capability of the model to correctly identify mapped landslides (TP; true positive), (2) the frequency of errors when mapped landslides are not correctly identified (FN; false
20 negative), (3) over-prediction (FP; false positive), and (4) the model's ability to correctly identify the area that does not include the mapped landslides (TN; true negative). An ideal landslide susceptibility map simultaneously maximises the agreement between the known and predicted landslide locations and minimises the area outside the known landslides that is predicted to be unstable (FP). To perform the ROC analysis, two
25 quantities were calculated: sensitivity (the true positive rate), defined as the ratio between TP and the sum of TP and FN, and specificity (the false positive rate), defined as the ratio between FP and the sum of TN and FP. Accuracy was defined as the ratio of TP+TN to the sum of all values (TP+FP+FN+TN) (Fig. 3). Relatively flat areas such

as rivers including alluvia, rice paddies, etc. were excluded from the analysis because the mapped shallow landslides only occurred in the mountainous area.

4 Results and discussion

4.1 Shallow landslide simulation using experimental data set (Case I)

The three different soil parameters (Table 1) used in the shallow landslide model for the 16 July 2006, event were further analysed to quantify the spatial discrepancy between the landslides triggered by the July 2006 rainfall event and the prediction results for the critical rainfall level that would trigger a shallow landslide in the area (Fig. 4). The resulting map of steady-state critical rainfall (mm day^{-1}) that could trigger shallow landslides in the study area is shown in Fig. 4, where the shallow landslide-prone areas predicted by Eq. (1) are delineated by the steady-state rainfall intensity (mm day^{-1}) necessary for slope instability in each topographic element. These were also compared with the shallow landslides observed in air photo images.

In Fig. 4a and b, which are based on the direct shear test data, the steady-state critical rainfall varied between 50 and 400 mm day^{-1} except in the stable area, and shallow landslides occurred near the high mountains in the simulated area. The landslide areas surveyed in 2006 showed a similar pattern to the critical rainfall simulation results, but these revealed an over-prediction, particularly around high mountain areas. The landslide occurrence based on triaxial compression test data also showed calculated critical rainfall levels at 50–400 mm day^{-1} except in the stable area (Fig. 4c). However, it was sensitive to rainfall levels of 50–200 mm day^{-1}, and most of the areas could be exposed to landslide risk when compared with mapped air photo images. Furthermore, in all three cases, the steep slope of the study area indicates relatively high possibility of a landslide triggered by a critical rainfall level of 0–50 mm day^{-1}.

We separated the steady-state critical rainfall (mm day^{-1}) data from the simulated grid data (Fig. 5) to obtain the distribution of steady-state critical rainfall levels

(mm day^{-1}) from the three types of experimental soil data. In Fig. 5, Cases I-a and I-b showed a large stable area (stable cells and cells > 400 mm day^{-1}), but Case I-c showed less than half the number of stable cells. The low values of Case I-c mean that the triaxial compression test soil data were more sensitive than the direct shear test soil data.

Following many other studies (e.g., Begueria, 2006b; Fawcett, 2006; Park et al., 2013), we performed ROC analysis to evaluate the accuracy of the modelling results. The calculated accuracy values of Cases I-a, I-b, and I-c were 0.71, 0.73, and 0.48, respectively. The ROC analysis indicated low overall model accuracy, with the accuracy of Case I-c (0.48) being the lowest of the three. The difference among the three cases can be attributed to the soil testing methods, specifically, the values for soil cohesion and internal friction angle that were determined by direct shearing and triaxial compression tests in this study.

Frank et al. (2009) observed that the triaxial compression test is better than the direct shear test for predictive models of shallow landslides, as it represents the processes and characteristics of the superficial soil layers reasonably well. Although we expected that the accuracy of the simulation-determined critical rainfall level for triggering shallow landslides for a model based on triaxial compression test data would be higher than one based on direct shear test data, the accuracy results for the three cases showed the opposite scenario. The triaxial compression test data (Case I-c) showed a clearly lower cohesion value and a slightly higher internal friction angle compared with Cases I-a and I-b (Table 1), which might have resulted in the low prediction accuracy of Case I-c.

Many researchers (e.g., Montgomery et al., 1998; Claessens et al., 2005; Ho et al., 2012; Uchida et al., 2011) have observed that the input parameters are prone to error in shallow landslide prediction models based on rainfall due to the sensitivity of certain parameters, particularly the internal friction angle and cohesion (Claessens et al., 2005; Roso et al., 2006; Uchida et al., 2011). Ho et al. (2012) also noted that the model results are affected by the influence of soil thickness and the development of vegeta-

tion on these parameters. Soil samples collected for laboratory testing do not reflect the root cohesion in situ. Soil weight can differ due to changes in soil thickness and/or soil cohesion that can be affected by soil thickness. Although soil samples were collected in the same study area and were tested using same methods, the results could differ among sampling locations. Therefore, soil cohesion and the friction angle of the slope materials were considered the major sources of uncertainty because of spatial variability and limited sampling (Chowdhury and Flentje, 2003; Xie et al., 2004; Shou and Chen, 2005; Huang et al., 2006; Griffiths et al., 2011).

4.2   Soil parameterisation and simulations (Cases II and III)

The total amount of water in a soil column is modulated by the local soil water-holding capacity and the transmissivity and topographic position of the soil. Local soil hydraulic properties are primarily related to soil grain size, root frequency, and soil composition (Casadei, 2003). Both the resistance of a root to tensile stress and the distribution of roots within a soil column are likely to be affected by plant responses to differences in climate and soil properties. Soil cohesion has sometimes been neglected in the stability analyses of steep slopes, whereas the angle of repose has purposely been increased to realistic values to account for the overall shear strength of aggregates (Montgomery and Dietrich, 1994; D'odorico and Fagherazzi; 2003). Therefore, soil cohesion is considered a sensitive parameter in shallow landslide models and is one of the most difficult parameters to quantify. The empirical treatment of the soil cohesion parameter can lead to large errors in the assessment of slope stability (Wooten et al., 2007; Kuriakose et al., 2013).

Bagherzadeh-Khalkhali and Mirghasemi (2009) and Ruiz-Villanueva et al. (2011) noted that experimental geotechnical tests on coarse-grained soils are generally difficult, and it is often necessary to remove large particles due to the dimensional limitations of laboratory specimens. Iida (1999) used the stochastic hydro-geomorphological model for the prediction of shallow landslides induced by rainstorms. He stated that the two-layer model of soil and bedrock, which assumes a potential landslide (soil) layer,

M. S. Kim et al.

is suitable for slope stability analysis in the context of shallow landslides. Following Iida (1999), we determined the shallow landslide distribution in the study area using Eqs. (6) and (7) to calculate physical soil parameters such as cohesion and internal friction angle. The assumptions of Eqs. (6) and (7) are that (1) shallow landslides only occurred when soil was completely saturated during a rainfall event and (2) shallow landslides only occurred between soil and bedrock (Fig. 6).

Using Eqs. (6) and (7) of the stochastic hydro-geomorphological model, the occurrence of shallow landslides was restricted to the area within the curves of D_{cr} and D_{max} in Fig. 6. The D_{cr} curve of the completely unsaturated state and the D_{max} curve of the fully saturated state (Fig. 6) were integral to determining the optimal cohesion and internal friction angle values. We are able to control the D_{cr} and D_{max} curves by controlling the internal friction angle and especially the cohesion. The distribution of soil thickness against slope angle is a very important input parameter when controlling the curves of D_{cr} and D_{max} for calculating the two soil parameters.

Figure 6 shows the results of soil parameterisation, which reflect the effect of soil thickness (i.e., the measured soil thickness in Fig. 2a and the average soil thickness of 1 m in Fig. 2a), using Eq. (6) (D_{cr}) and Eq. (7) (D_{max}) in the hydro-geomorphological model derived from the soil parameters in Table 1. Figure 6a (Case I) shows an overlap with the distribution of measured soil thickness (y axis) against the slope angle (x axis) (black circles are located within the shallow landslide scar, and white circles are located external to the shallow landslide scar). The curves (D_{cr}) and (D_{max}) were calculated using the data in Table 1. The black circles are located outside D_{cr} and D_{max}, indicating that the cohesion and internal friction values used in the Case I simulation for shallow landslide prediction in Fig. 4 contain errors. Accordingly, we changed the internal friction angle and cohesion values, resulting in values nested between D_{cr} and D_{max} in Fig. 6 for Cases II and III.

Case II (Fig. 6) shows an overlap with the distribution of measured soil thickness (y axis) against slope angle (x axis), and the curves were controlled using changes in the internal friction angle and cohesion. Case III (Fig. 6) shows an overlap with the

distribution of the average soil thickness (1 m) (y axis) against slope angle (x axis), and the curves were also controlled using changes in the internal friction angle and cohesion.

All values calculated by the hydro-geomorphological model are presented in Table 3. The internal friction angle and cohesion values in Table 3 were greater than those listed in Table 1. In particular, the soil cohesion value determined by triaxial compression test (Table 1) was almost doubled due to the influence of soil thickness (Table 3).

To evaluate the effect of soil thickness on the soil parameters we applied altered soil parameters to the SHALSTAB model (i.e., measured soil thickness (Case II) and a constant soil thickness of 1 m (Case III)), and steady-state critical rainfall (mm day^{-1}) was re-calculated for shallow landslide prediction. The accuracy of this shallow landslide prediction was also evaluated using ROC analysis to assess any improvement in the prediction accuracy compared with the results for Case I.

Figure 7 shows the distribution of the areas with rainfall values critical for the occurrence of shallow landslides. Figure 7a (Case II-a) and Fig. 7b (Case II-b) show the critical rainfall distribution using soil parameters from the direct shear test, incorporating the effect of measured soil thickness distribution (Table 3). Figure 7c (Case II-c) shows the critical rainfall distribution using soil parameters from the triaxial compression test, incorporating the effect of measured soil thickness distribution (Table 3). The critical rainfall simulation results in Fig. 7 were compared with the shallow landslide grid derived from air photo images from a post-event survey of the study area in 2006.

The distribution of the simulated critical rainfall (mm day^{-1}) in Fig. 7a and b based on the results for Cases II-a and II-b (Fig. 6 and Table 3) showed a similar pattern to the air photo images grid (red colour). The simulated critical rainfall values in Fig. 7a and b showed that the area of unconditionally stable cells increased. The critical rainfall values were 0–50 mm day^{-1}, which show decreased sensitivity for shallow landslide occurrence compared with Fig. 4a and b. Figure 7c shows the distribution of simulated critical rainfall (mm day^{-1}) based on the results for Case II-c (Fig. 6 and Table 3), and also shows a similar pattern to the air photo images grid (red colour). However, the

critical rainfall simulation results in Fig. 7c differ from those in Fig. 7a and b. In Fig. 7c, the area of unconditionally stable cells increased, similar to those in Fig. 7a and b, but the critical rainfall value increased to over 400 mm day^{-1}. The distribution of critical rainfall in Fig. 7c matched well with the shallow landslide locations of 2006.

5 The distributions of the critical rainfall simulation using soil parameters reflected effects of measured soil thickness in Fig. 6 (Case II); the grid cells simulated in Fig. 7 are presented in Fig. 8. The distribution patterns of critical rainfall cells in Cases II-a and II-b (Fig. 8) were similar, and the number of stable cells increased, in contrast to Cases I-a and I-b, (Fig. 5) based on the direct shear test method. The distribution of critical
10 rainfall cells in Case II-c (Fig. 8) showed that stable cells and cells of > 400 mm increased, in contrast to Case I-c (Fig. 5), based on the triaxial compression test method. This means that the over-prediction of shallow landslide occurrence under light rainfall conditions decreased.

To evaluate the impact of soil parameters other than soil thickness, we performed

The accuracy of the simulated critical rainfall prediction for Case II was evaluated
15 by ROC analysis. The ROC analysis values for Case II are presented in Table 4. The ROC accuracy values for Cases II-a, II-b, and II-c were 0.83, 0.86, and 0.85, respectively. All simulation cases in Fig. 7, simulating the distribution of critical rainfall values (mm day^{-1}), clearly improved over those of Case I (Fig. 4). ROC analysis results are presented in Table 4; the increased ROC values for Case II (Fig. 7) indicate improved
20 predictive accuracy for the critical rainfall simulation. This also demonstrates that soil cohesion and internal friction angle may be important factors for shallow landslide modelling.

To evaluate the impact of soil parameters other than soil thickness, we performed shallow landslide simulation using an average soil thickness of 1 m (Case III in Fig. 6
25 and Table 3). The critical rainfall simulation distribution for the effect of 1 m soil thickness on shallow landslide occurrence is shown in Fig. 9. The distribution of the critical rainfall value in Fig. 9a (Case III-a) was similar to that of Case II-a (Fig. 7), but it differed from the other cases in Fig. 9. The critical rainfall values of < 50 mm day^{-1} (Fig. 9b) and 100–200 mm day^{-1} (Fig. 9c), were low, which differed from the sensitivity in Fig. 7. The low

sensitivities of Cases III-b and III-c in Fig. 9 mean that soil cohesion and the internal friction angle can still influence the outcome of the critical rainfall simulation despite a constant average soil thickness of 1 m.

The distribution of simulated critical rainfall cells (Fig. 9) is presented in Fig. 10. The distribution patterns for Cases III-a and III-c are similar (Fig. 10). However, the critical rainfall cells in Case III-b (Fig. 10) show that the distribution of $< 50\,\mathrm{mm\,day^{-1}}$ cells increased and stable cells decreased compared with the other simulations (Fig. 10).

The critical rainfall simulation accuracy of Fig. 10 was evaluated by ROC analysis and is presented in Table 4. The accuracy values for Cases III-a, III-b, and III-c were calculated as 0.83, 0.79, and 0.78, respectively. The accuracy values of Case III were higher than those of Case I (Fig. 4), but lower than those of Case II (Fig. 7). Therefore, the accuracy of the shallow landslide prediction based on ROC analysis follows Case II > Case III > Case I. This indicates that soil parameterisation using soil thickness is important for improving the shallow landslide prediction accuracy of a model. These soil parameters (i.e., internal friction angle and soil cohesion) can greatly affect the prediction of shallow landslides.

Recent studies have dealt with the effects of soil cohesion and internal friction angle on slope stability analyses (e.g. Low and Tang, 1997; Liang et al., 1999; Cherubini, 2000; Hong and Roh, 2008; Cho, 2010; Cho and Park, 2010). According to Montgomery and Dietrich (1994), the effect of roots on shear stress resistance was taken into account by increasing the value of the internal friction angle by 40 %. Schmidt et al. (2001) and D'Odorico and Fagherazzi (2003) observed that soil and root cohesion are inherently necessary to build up soil in steep hollows, otherwise landslides would occur even with light rainfall. Additionally, Slide and Ochiai (2006) noted that observations of shallow landslides in certain areas indicate the existence of a threshold soil thickness for some slopes and soil properties, beyond which failure must occur, provided that the slope gradient is greater than the internal friction angle of the failure surface. However, we determined that the relationships among the internal friction an-

gle, soil cohesion, and soil depth are important for improving the accuracy of shallow landslide prediction.

4.3 Effect of topography on the accuracy of prediction, and its limitations

Figures 7 and 9 show the shallow landslide prediction results using soil parameterisation representing the effects of measured (Case II) and average (Case II) soil thickness (Fig. 6). Shallow landslide predictions using soil parameterisation showed greater accuracy than those using experimental soil parameters (Case I) (Fig. 4).

The order of shallow landslide prediction accuracy based on ROC analysis was Case II > Case III > Case I. Although we performed soil parameterisation for shallow landslide prediction, over-prediction was still detected (Fig. 7). There are many reasons for such over-prediction in this study. Antecedent rainfall and DEM effects could be the primary factors resulting in over-prediction. Due to the difficulty of performing field tests for hydraulic conductivity (K_s) on high steep mountainous slopes, classical methods for measuring hydraulic conductivity have involved the laboratory test-based "constant head" and "falling head" parameters using soil core samples extracted from the field. Eq. (1) assumes steady-state hydraulic conductivity, meaning that antecedent rainfall is not considered. Antecedent rainfall plays an important role in the initiation of landslides (Wieczorek, 1987), but its influence is difficult to quantify. Soil water conditions from antecedent rainfall depend on several factors including local climatic conditions, slope angle, and the heterogeneity of the physical–mechanical properties and permeability of the soil (Aleotti, 2004). Therefore, we were unable to determine the in situ soil water conditions, and instead used the steady-state critical rainfall obtained from the SHALSTAB model.

We used a 5 m-resolution DEM with a 5 m contour digital map (see Sect. 3.3) for shallow landslide prediction. We were unable to investigate the effect of DEM resolution in this study, but several authors (e.g., Zhang and Montgomery, 1994; Clasessens et al., 2005; Penna et al., 2014) have previously analysed the effect of DEMs on modelling results.

Claessens et al. (2005) calculated steady-state critical rainfall using different DEM resolutions and observed that even using high-resolution DEMs such as LIDAR data for shallow landslide prediction modelling, the model cannot describe the characteristics of the natural hillslope in detail. Many previous studies (e.g., Claessens et al., 2005; Tarolli and Tarboton, 2006) concluded that even if high-resolution DEMs are used to analyse shallow landslides, the complete prediction of the shallow landslide area is difficult. To increase the accuracy of shallow landslide prediction, we performed soil parameterisations using three kinds of experimental soil data (two direct shear tests and one triaxial compression test) and applied them to a stochastic hydro-geomorphological model based on soil thickness. We achieved a more accurate critical rainfall modelling result for rainfall-induced shallow landslide prediction than that obtained prior to soil parameterisation. Although we only considered physical soil properties in this study, further study of other factors including the effects of hydraulic conductivity and antecedent rainfall will be needed to improve shallow landslide prediction.

5   Conclusions

The study site in S. Korea is the ideal field site to evaluate the shallow landslide prediction because the shallow landslides occurrence is only caused by the recently increased heavy rainstorms. To improve the accuracy of shallow landslide prediction, we compared the results of shallow landslide predictions using a SHALSTAB model, varying the input soil data. Experimental soil data were used for the first simulation (Case I), whereas soil data represented the measured soil thickness (Case II) and represented average soil thickness (1 m, Case III) data were used in the second and third simulations, respectively. The accuracy of shallow landslide prediction was evaluated by ROC analysis. The order of accuracy as determined by ROC analysis was Case II > Case III > Case I, indicating that Case II showed the highest predictive accuracy. Therefore, the use of soil properties reflecting soil thickness may improve the accuracy of shallow landslide prediction. Soil parameterisation can help to improve the accuracy of pre-

diction, but further study of hydraulic conductivity as affected by antecedent rainfall is needed.

Author contributions. M. S. Kim and J. K. Kim carried out the experiments and performed the simulations. Y. Onda gave the idea and designed the experiments. All co-authors discussed the results from the simulations. M. S. Kim prepared the manuscript with contributions from all co-authors.

References

Aleotti, P.: A warning system for rainfall-induced shallow failures, Eng. Geol., 73, 247–265, 2004.

Anderson, M. G. and Kemp, M. J.: Towards an improved specification of slope hydrology in the analysis of slope instability problems in the tropics, Prog. Phys. Geog., 15, 29–52, 1991.

Anderson, S. A. and Reimer, M. F.: Collapse of saturated soil due to reduction in confinement, J. Geotech. Eng.-ASCE, 121, 216–220, 1995.

Anderson, S. A. and Sitar, N.: Analysis of rainfall-induced debris flows, J. Geotech. Eng.-ASCE, 121, 544–552, 1995.

Bagherzadeh-Khalkhali, A. and Mirghasemi, A. A.: Numerical and experimental direct shear tests on coarse-grained soils, Particuology, 7, 83–91, 2009.

Beguería, S.: Validation and evaluation of predictive models in hazard assessment and risk management, Nat. Hazards, 37, 315–329, 2006.

Borga, M., Dalla Fontana, G., Gregoretti, C., and Marchi, L.: Assessment of shallow landsliding by using a physically based model of hillslope stability, Hydrol. Process., 16, 2833–2851, 2002.

Caine, N.: The rainfall intensity-duration control of shallow landslides and debris flows, Geogr. Ann. A, 62, 23–27, 1980.

Campbell, R. H.: Soil slips, debris flows, and rainstorms in the Santa Monica Mountains and Vicinity, Southern California, USGS, Prof. Paper 851, US Govern. Print, Washington, 1–20, 1975.

Cannon, S. H., Gartner, J. E., Wilson, R. C., Bowers, J. C., and Laber, J. L.: Storm rainfall conditions for floods and debris flows from recently burned areas in southwestern Colorado and southern California, Geomorphology, 96, 250–269, 2008.

Casadei, M., Dietrich, W. E., and Miller, N. L.: Testing a model for predicting the timing and location of shallow landslide initiation in soil mantled landscapes, Earth Surf. Proc. Land., 28, 925–950, 2003.

Cherubini, C.: Reliability evaluation of shallow foundation bearing capacity on c' and ϕ' soils, Can. Geotech. J., 37, 264–269, 2000.

Cho, S. E.: Probabilistic assessment of slope stability that considers the spatial variability of soil properties, J. Geotech. Geoenviron., 136, 975–984, 2010.

Cho, S. E. and Park, H. C.: Effect of spatial variability of cross-correlated soil properties on bearing capacity of strip footing, Int. J. Numer. Anal. Meth., 34, 1–26, 2010.

Chowdhury, R. and Flentje, P.: Role of slope reliability analysis in landslide risk management, B. Eng. Geol. Environ., 62, 41–46, 2003.

Claessens, L., Heuvelink, G. B. M., Schoorl, J. M., and Veldkamp, A.: DEM resolution effects on shallow landslide hazard and soil redistribution modeling, Earth Surf. Proc. Land., 30, 461–477, 2005.

Coe, J. A., Kinner, D. A., and Godt, J. W.: Initiation conditions for debris flows generated by runoff at Chalk Cliffs, Central Colorado, Geomorphology, 96, 270–297, 2008.

Crosta, G. B. and Dal Negro, P.: Observations and modelling of soil slip-debris flow initiation processes in pyroclastic deposits: the Sarno 1998 event, Nat. Hazards Earth Syst. Sci., 3, 53–69, doi:10.5194/nhess-3-53-2003, 2003.

Crosta, G. B. and Frattini, P.: Distributed modelling of shallow landslides triggered by intense rainfall, Nat. Hazards Earth Syst. Sci., 3, 81–93, doi:10.5194/nhess-3-81-2003, 2003.

Dietrich, W. E. and Montgomery, D. R.: SHALSTAB – a Digital Terrain Model for Mapping Shallow Landslide Potential, National Council of the Paper Industry for Air and Stream Improvement, Technical Report, Berkeley, 29 February, 1998.

Dietrich, W. E., Reiss, R., Hsu, M., and Montgomery, D. R.: A process-based model for colluvial soil depth and shallow landsliding using digital elevation data, Hydrol. Process., 9, 383–400, 1995.

Improvement of shallow landslide prediction accuracy using soil parameterisation

M. S. Kim et al.

Title Page

Abstract	Introduction
Conclusions	References
Tables	Figures

◄◄   ►►

◄   ►

Back   Close

Full Screen / Esc

Printer-friendly Version

Interactive Discussion

D'Odorico, P. and Fagherazzi, S.: A probabilistic model of rainfall-triggered shallow landslides in hollows: a long-term analysis, Water Resour. Res., 39, 1262, doi:10.1029/2002WR001595, 2003.

Eyles, R. J., Crozier, M. J., and Wheeler, R. H.: Landslips in Wellington City, New Zeal. Geogr., 34, 58–74, 1978.

Fawcett, T.: An introduction to ROC analysis, Pattern Recogn. Lett., 27, 861–874, 2006.

Fernandes, N. F., Guimarães, R. F., Gomes, R. A. T., Vieira, B. C., Montgomery, D. R., and Greenberg, M. H.: Topographic controls of landslides in Rio de Janeiro: field evidence and modeling, Catena, 55, 163–181, 2004.

Gabet, E. J. and Mudd, S. M.: The mobilization of debris flows from shallow landslides, Geomorphology, 74, 207–218, 2006.

Graf, F., Frei, M., and Böll, A.: Effects of vegetation on the angle of internal friction of a moraine, For. Snow and Landsc. Res., 82, 61–77, 2009.

Giannecchini, R.: Relationship between rainfall and shallow landslides in the southern Apuan Alps (Italy), Nat. Hazards Earth Syst. Sci., 6, 357–364, doi:10.5194/nhess-6-357-2006, 2006.

Giannecchini, R., Naldini, D., D'Amato Avanzi, G., and Puccinelli, A.: Modelling of the initiation of rainfall-induced debris flows in the Cardoso basin (Apuan Alps, Italy), Quatern. Int., 171, 108–117, 2007.

Godt, J. W. and McKenna, J. P.: Numerical modeling of rainfall thresholds for shallow landsliding in the Seattle, Washington, area, in: Landslides and Engineering Geology of the Seattle Washington Area, edited by: Baum, R. L., Godt, J. W., Highland, L. M., Geol. Soc. Am. Rev. in Engi. Geol., 20, 121–136, doi:10.1130/2008.4020(07), 2008.

Godt, J. W., Baum, R. L., Savage, W. Z., Salciarini, D., Schulz, W. H., and Harp, E. L.: Transient deterministic shallow landslide modeling: requirements for susceptibility and hazard assessments in a GIS framework, Eng. Geol., 102, 214–226, 2008.

Griffiths, D. V., Huang, J., and Fenton, G. A.: Probabilistic infinite slope analysis, Comput. Geotech., 38, 577–584, 2011.

Guthrie, R. H.: The effects of logging on frequency and distribution of landslides in three watersheds on Vancouver Island, British Columbia, Geomorphology, 43, 273–292, 2002.

Guzzetti, F., Peruccacci, S., Rossi, M., and Stark, C. P.: Rainfall thresholds for the initiation of landslides in central and southern Europe, Meteorol. Atmos. Phys., 98, 239–267, 2007.

Discussion Paper | Discussion Paper | Discussion Paper | Discussion Paper |

Guzzetti, F., Peruccacci, S., Rossi, M., and Stark, C. P.: The rainfall intensity-duration control of shallow landslides and debris flows: an update, Landslides, 5, 3–17, 2008.

Ho, J. Y., Lee, K. T., Chang, T. C., Wang, Z. Y., and Liao, Y. H.: Influence of spatial distribution of soil thickness on shallow landslide prediction, Eng. Geol., 124, 38–46, 2012.

Hong, H. P. and Roh, G.: Reliability evaluation of earth slope, J. Geotech. Geoenviron., 134, 1700–1705, 2008.

Hong, S. H., Hwang, S. K., and Cho, D. R.: Geological report of the Changdong sheets, Korea Institute of Geoscience and Mineral Resources, Daejeon, 1995.

Jr-Chuan Huang, Shuh-Ji Kao, Mei-Ling Hsu, and Jiun-Chuan Lin: Stochastic procedure to extract and to integrate landslide susceptibility maps: an example of mountainous watershed in Taiwan, Nat. Hazards Earth Syst. Sci., 6, 803–815, doi:10.5194/nhess-6-803-2006, 2006.

Iida, T.: A stochastic hydro-geomorphological model for shallow landsliding due to rainstorm, Catena, 34, 293–313, 1999.

Iverson, R. M.: Landslide triggering by rain infiltration, Water Resour. Res., 36, 1897–1910, 2000.

Iverson, R. M., Reid, M. E., and LaHusen, R. G.: Debris-flow mobilization from landslides, Annu. Rev. Earth Pl. Sc., 25, 85–138, 1997.

Kuriakose, S. L., van Beek, L. P. H., and van Westen, C. J.: Parameterizing a physically based shallow landslide model in a data poor region, Earth Surf. Proc. Land., 34, 867–881, 2009.

Lee, M. S., Ryu, J. C., and Kim, K. S.: Development of the Linear Regression Analysis Model to estimate the shear strength of soils, J. Eng. Geol. Korea, 19, 177–189, 2009.

Lee, K. T. and Ho, J. Y.: Prediction of landslide occurrence based on slope-instability analysis and hydrological model simulation, J. Hydrol., 375, 489–497, 2009.

Liang, W. L. and Uchida, T.: Effects of topography and soil depth on saturated-zone dynamics in steep hillslopes explored using the three-dimensional Richards' equation, J. Hydrol., 510, 124–136, 2013.

Low, B. K. and Tang, W. H.: Efficient reliability evaluation using spreadsheet, J. Eng. Mech.-ASCE, 123, 749–752, 1997.

Montgomery, D. R. and Dietrich, W. E.: A physically based model for the topographic control on shallow landsliding, Water Resour. Res., 30, 1153–1171, 1994.

Montgomery, D. R., Dietrich, W. E., Torres, R., Anderson, S. P., and Loague, K.: Subsurface flow paths in a steep unchannelled catchment, Water Resour. Res., 33, 91–109, 1997.

Improvement of shallow landslide prediction accuracy using soil parameterisation

M. S. Kim et al.

Montgomery, D. R., Sullivan, K., and Greenberg, M. H.: Regional test of a model for shallow landsliding, Hydrol. Process., 12, 943–955, 1998.

Montgomery, D. R., Schmidt, K. M., Green Berg, H. M., and Dietrich, W. E.: Forest clearing and regional landsliding, Geology, 28, 311–314, 2000.

5 Montgomery, D. R., Balco, G., and Willett, S. D.: Climate, tectonics, and the morphology of the Andes, Geology, 29, 579–582, doi:10.1130/0091-7613(2001)029<0579:CTATMO>2.0.CO;2, 2001.

O'Loughlin, E. M.: Prediction of surface saturation zones in natural catchments by topographic analysis, Water Resour. Res., 22, 794–804, 1986.

10 Park, H. J., Lee, J. H., and Woo, I. K.: Assessment of rainfall-induced shallow landslide susceptibility using a GIS-based probabilistic approach, Eng. Geol., 161, 1–15, 2013.

Penna, D., Borga, M., Aronica, G. T., Brigandì, G., and Tarolli, P.: The influence of grid resolution on the prediction of natural and road-related shallow landslides, Hydrol. Earth Syst. Sci., 18, 2127–2139, doi:10.5194/hess-18-2127-2014, 2014.

15 Reid, M. E., LaHunsen, R. G., and Iverson, R. M.: Debris flow initiation experiments using diverse hydrologic triggers, in: Debris Flow Hazards Mitigation: Mechanics, Prediction and Assessment, edited by: Chen, C. L., Proceedings of first international conference (7–9 August 1997), San Francisco, CA. New York, NY, American Society of Civil Engineers, 1–11, 1997.

20 Reid, M. E., Christian, S. B., and Brien, D. L.: Gravitational stability of three-dimensional stratovolcano edifices, J. Geophys. Res., 105, 6043–6056, 2000.

Reid, L. M. and Page, M. J.: Magnitude and frequency of landsliding in a large New Zealand catchment, Geomorphology, 49, 71–88, 2002.

Reimer, M. F.: The effects of testing conditions on the constitutive behavior of loose, saturated
25 sands under monotonic loading, Ph.D. thesis, University of California, Berkeley, 1992.

Rickenmann, D. and Zimmermann, M.: The 1987 debris flows in Switzerland: documentation and analysis, Geomorphology, 8, 175–189, 1993.

Rosso, R., Rulli, M. C., and Vannucchi, G.: A physically based model for the hydrologic control on shallow landsliding, Water Resour. Res., 42, W06410, doi:10.1029/2005WR004369,
30 2006.

Ruiz-Villanueva, V., Bodoque, J. M., Díez-Herrero, A., and Calvo, C.: Triggering threshold precipitation and soil hydrological characteristics of shallow landslides in granitic landscapes, Geomorphology, 133, 178–189, 2011.

Schmidt, K. M., Roering, J. J., Stock, J. D., Dietrich, W. E., Montgomery, D. R., and Shaub, T.: Root cohesion variability and shallow landslide susceptibility in the Oregon Coast Range, Can. Geotech. J., 38, 995–1024, 2001.

Selby, M. J.: Slope erosion due to extreme rainfall: a case study from New Zealand, Geogr. Ann., 3A, 131–138, 1976.

Sidle, R. C. and Ochiai, H.: Landslides: Processes, Prediction, and Land Use, Am. Geophys. Union, Washington DC, 312, 2006.

Shou, K. J. and Chen, Y. L.: Spatial risk analalysis of the Li-shan landslide in Taiwan, Eng. Geol., 80, 199–213, 2005.

Swets, J. A.: Measuring the accuracy of diagnostic systems, Science, 240, 1285–1293, 1988.

Talebi, A., Troch, P. A., and Uijlenhoet, R.: A steady-state analytical hillslope stability model for complex hillslopes, Hydrol. Process., 22, 546–553, 2008

Tarolli, P. and Tarboton, D. G.: A new method for determination of most likely landslide initiation points and the evaluation of digital terrain model scale in terrain stability mapping, Hydrol. Earth Syst. Sci., 10, 663–677, doi:10.5194/hess-10-663-2006, 2006.

Uchida, T., Mori, N., Tamura, K., Takiguchi, S., and Kamee, K.: The role of data preparation on shallow landslide prediction, J. Jap. Soc. Eros. Cont. Eng., 62, 23–31, 2009

Uchida, T., Tamur, K., and Akiyama, K.: The role of grid cell size, flow routing algorithm and spatial variability of soil depth on shallow landslide prediction, Ital. J. Eng. Geol. Environ., 11, 149–157, doi:10.4408/IJEGE.2011-03.B-018, 2011.

Van Den Eeckhaut, M., Vanwalleghem, T., Poesen, J., Govers, G., Verstraeten, G., and Vandekerckhove, L.: Prediction of landslide susceptibility using rare events logistic regression: a case study in the Flemish Ardennes (Belgium), Geomorphology, 76, 392–410, doi:10.1016/j.geomorph.2005.12.003, 2006.

Vanacker, V., Vanderschaeghe, M., Govers, G., Willems, E., Poesen, J., Deckers, J., and De Bievre, B.: Linking hydrological, infinite slope stability and land-use change models through GIS for assessing the impact of deforestation on slope stability in high Andean watersheds, Geomorphology, 52, 299–315, 2003.

Wieczorek, G. F.: Effect of rainfall intensity and duration on debris flows in central Santa Cruz Mountains, California, in: Debris Flows/Avalanches: Processes, Recognition and Mitigation, edited by: Costa, J. E. and Wieczorek, G. F., Reviews in Eng. Geol., Geol. Soc. of Am., 7, 23–104, 1987.

Improvement of shallow landslide prediction accuracy using soil parameterisation

M. S. Kim et al.

Title Page

Abstract | Introduction

Conclusions | References

Tables | Figures

◀ | ▶

◀ | ▶

Back | Close

Full Screen / Esc

Printer-friendly Version

Interactive Discussion

Wilkinson, P. L., Anderson, M. G., Lloyda, D. M., and Renaudb, J. P.: Landslide hazard and bioengineering: towards providing improved decision support through integrated numerical model development, Environ. Modell. Softw., 17, 333–344, 2002.

Wu, W. and Sidle, R. C.: A distributed slope stability model for steep forested basins, Water Resour. Res., 31, 2097–2110, 1995.

Xie, M., Esaki, T., and Zhou, G.: GIS-based probabilistic mapping of landslide hazard using a three dimensional deterministic model, Nat. Hazards, 33, 265–282, 2004.

Yoshinaga, S. and Ohnuki, Y.: Estimation of soil physical properties from a handy dynamic cone penetrometer test, J. Jap. Soc. of Eros. Cont. Eng., 48, 22–28, 1995 (in Japanese with English abstract).

Zhang, W. and Montgomery, D. R.: Digital elevation model grid size, landscape representation, and hydrologic simulations, Water Resour. Res., 30, 1019–1028, 1994.

Zizioli, D., Meisina, C., Valentino, R., and Montrasio, L.: Comparison between different approaches to modeling shallow landslide susceptibility: a case history in Oltrepo Pavese, Northern Italy, Nat. Hazards Earth Syst. Sci., 13, 559–573, doi:10.5194/nhess-13-559-2013, 2013.

Improvement of shallow landslide prediction accuracy using soil parameterisation

M. S. Kim et al.

Table 1. Soil parameters for shallow landslide modelling (Case I and Case II were determined by direct shear test, and Case III was determined by triaxial compression test).

Model input parameters	Case I-a	Case I-b	Case I-c
Saturated soil weight ($kg\,m^{-3}$)	1790	1960	1740
Dry density ($kg\,m^{-3}$)	1550	1510	1490
Water density ($kg\,m^{-3}$)	1000	1000	1000
Hydraulic conductivity ($m\,h^{-1}$)	0.08	0.04	0.05
Cohesion (kPa)	3.8	4	1.6
Internal Friction Angle (°)	35.2	34	36.5
Slope degree (°)	DEM	DEM	DEM
Gravity velocity ($m\,s^{-1}$)	9.8	9.8	9.8
Average soil depth (m)	1 m	1 m	1 m

Table 2. Accuracy analysis of shallow landslide prediction using ROC analysis.

Model Class	True Positive Rate	False Positive Rate	False Negative	Accuracy
CASE I-a	0.37	0.28	0.63	0.71
CASE I-b	0.35	0.26	0.65	0.73
CASE I-c	0.65	0.52	0.35	0.48

Table 3. Soil property calculation results from the stochastic hydrogeomorphological model (Measured soil thickness data were used for Case II, and average soil thickness data were used for Case III).

Model input parameters	Case II-a	Case II-b	Case II-c	Case III-a	Case III-b	Case III-c
Saturated soil density ($kg\,m^{-3}$)	1790	1960	1740	1790	1960	1740
Dry density ($kg\,m^{-3}$)	1550	1510	1490	1550	1510	1490
Water density ($kg\,m^{-3}$)	1000	1000	1000	1000	1000	1000
Hydraulic conductivity ($m\,h^{-1}$)	0.08	0.08	0.04	0.04	0.05	0.05
Cohesion (kPa)	4.5	3.2	3.2	3.5	3.2	3.2
Internal Friction Angle (°)	37	34	37.2	37	34	37.2
Slope degree (°)	DEM	DEM	DEM	DEM	DEM	DEM
Gravity velocity ($m\,s^{-1}$)	9.8	9.8	9.8	9.8	9.8	9.8
Soil depth (m)	Measured	Measured	Measured	Average 1 m	Average 1 m	Average 1 m

Full Screen / Esc

Printer-friendly Version

Interactive Discussion

Table 4. ROC accuracy analysis of shallow landslide prediction using soil parameterisation for two soil thickness parameters (measured soil thickness and average soil thickness of 1 m).

Soil Thickness data	Simulation case	True Positive Rate	False Positive Rate	False Negative	Accuracy
Measured soil depth (m)	CASE II-a	0.30	0.16	0.70	0.83
	CASE II-b	0.16	0.13	0.84	0.86
	CASE II-c	0.32	0.14	0.68	0.85
Average soil depth (1 m)	CASE III-a	0.27	0.15	0.73	0.84
	CASE III-b	0.30	0.20	0.70	0.79
	CASE III-c	0.34	0.21	0.66	0.78
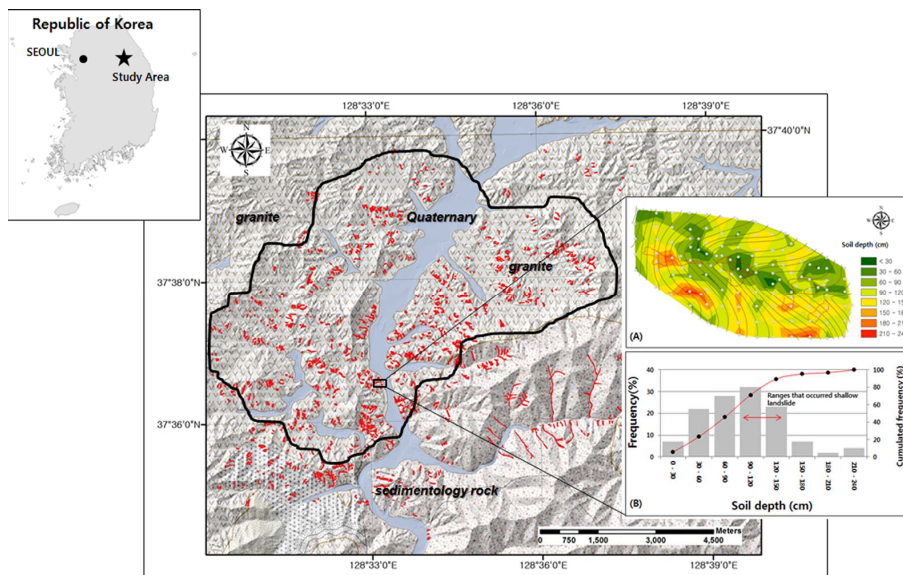
Figure 1. Location and lithology map of the study site. Red indicates areas covered by shallow landslides that occurred on 16 July 2006. (A) soil thickness distribution and (B) histogram of soil depths measured by penetration tests for 125 points in a small watershed within the landslide study area.
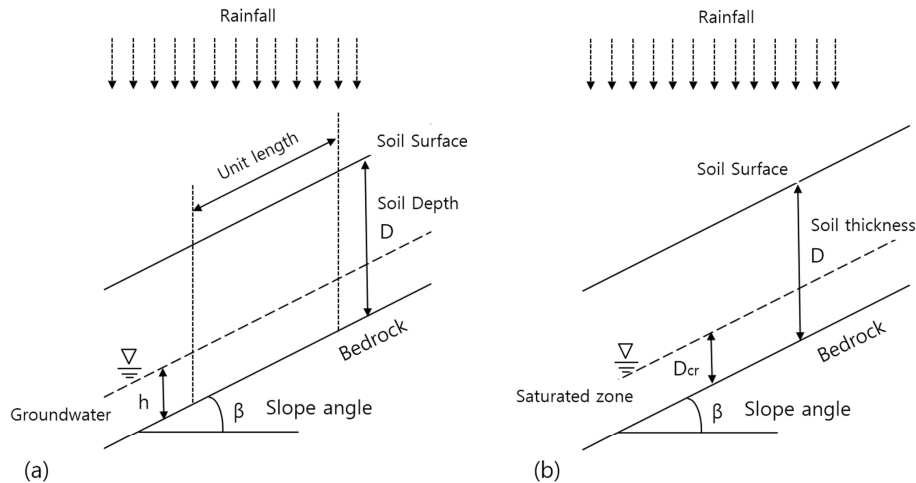
Figure 2. SHALSTAB **(a)** and stochastic hydro-geomorphology conceptual models **(b)**.

Figure 3. Reciever operating characteristic (ROC) analysis method for determining the accuracy of shallow landslide prediction in this study (modified from Godt et al., 2008).
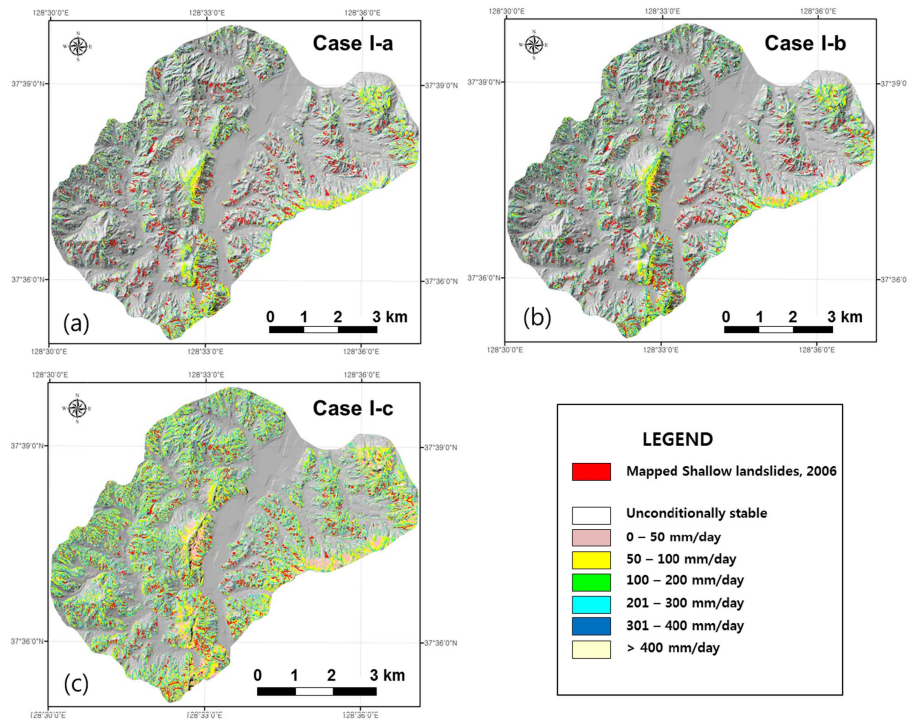
Figure 4. Maps of study area showing steady-state rainfall intensity (mm d^{-1}) necessary for slope instability as predicted from Eq. (1) using several soil parameters tested by direct shear test and triaxial compression test (Table 1) for the shallow landslide-prone area. Observed shallow landslides (in red) that occurred on 16 July 2006, are also shown mapped shallow landslides.
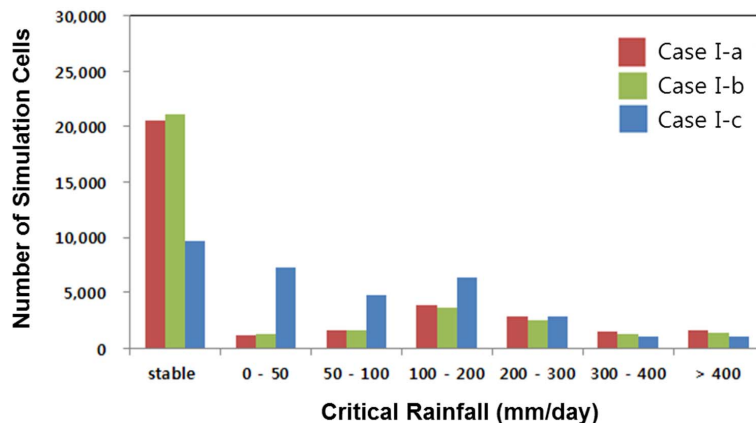
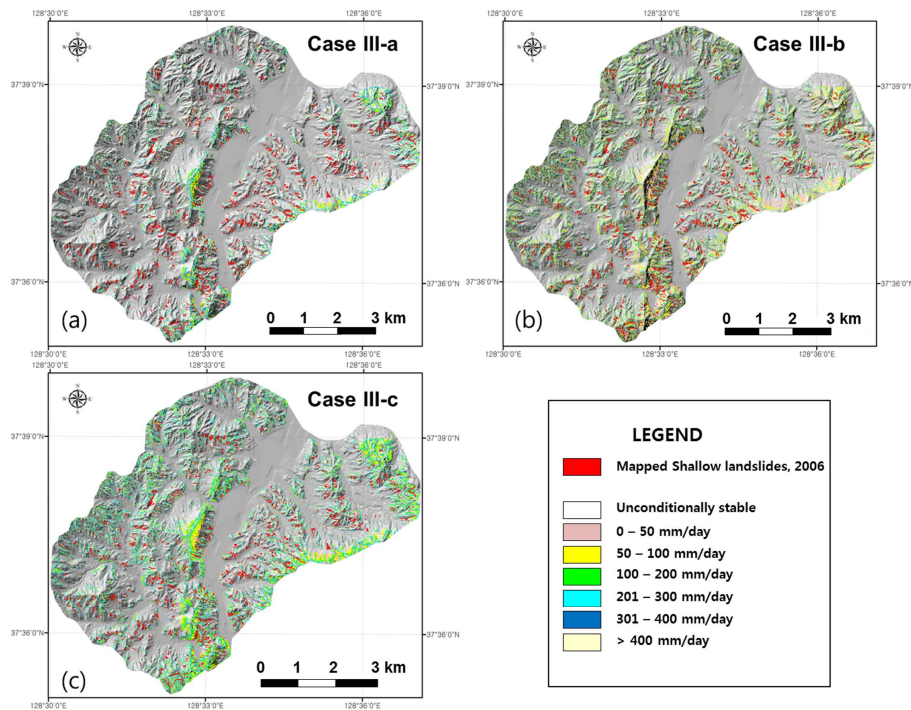**Figure 5.** Number of simulated cells and the distribution of critical rainfall intensity ($mm\,day^{-1}$) for Case I from the shallow landslide prediction based on the three soil parameters in Table 1.
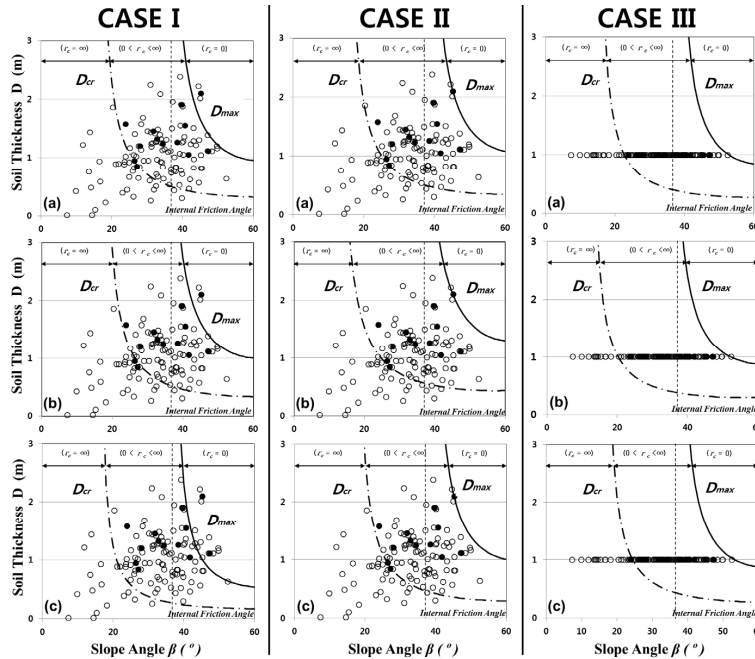
Figure 6. D_{cr} (dashed line) and D_{max} (solid line) calculated using Eqs. (6) and (7). Shallow landslides can occur between D_{cr} and D_{max}. White circles indicate soil thickness measured by knocking pole test outside of the shallow landslide area, and black circles indicate soil thickness measured by knocking pole test inside the shallow landslide scar. Case I was calculated using soil thickness and soil data shown in Table 1. Case II was calculated using soil thickness and by controlling the cohesion and internal friction angle based on data shown in Table 1. Case III was calculated using the average soil thickness and controlling for the cohesion and internal friction angle based on data shown in Table 1.

Full Screen / Esc

Printer-friendly Version

Interactive Discussion
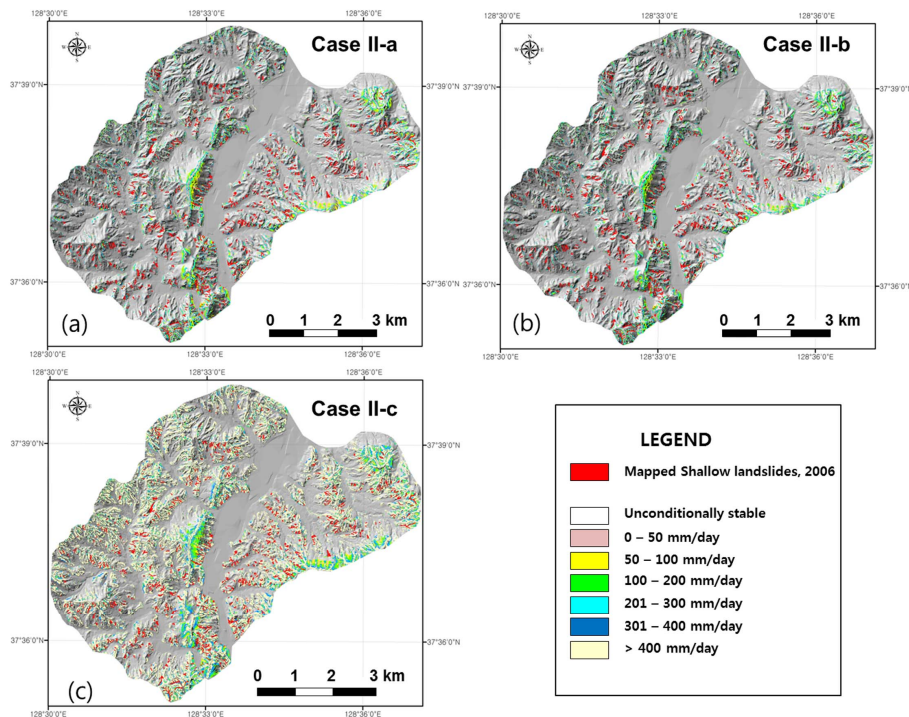
Figure 7. Maps of the simulation results showing the shallow landslide-prone areabased on the steady-state rainfall intensity ($mm\,d^{-1}$) necessary for slope instability as predicted from Eq. (1) using measured soil thickness (Table 1).
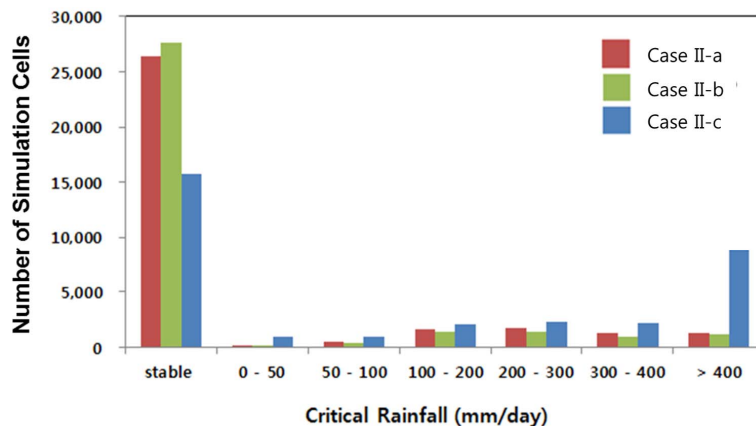
Figure 8. Number of simulated cells and the distribution of critical rainfall intensity (mm day^{-1}) for Case II from the shallow landslide prediction based on the three soil parameters in Table 1.

Figure 9. Maps of the simulation results showing the shallow landslide-prone areabased on the steady-state rainfall intensity ($mm\,d^{-1}$) necessary for slope instability as predicted from Eq. (1) using measured soil thickness (Table 3).
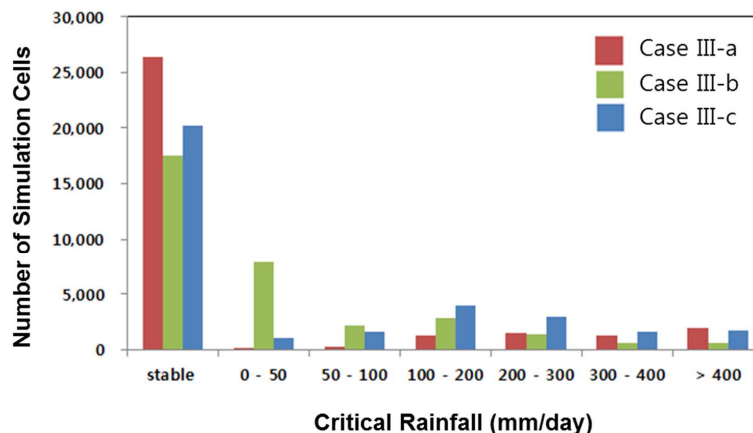
Figure 10. Number of simulated cells and the distribution of critical rainfall intensity (mm day^{-1}) for Case III from the shallow landslide prediction based on the three soil parameters in Table 3.